Nonlinear Dyn (2023) 111:391–410
https://doi.org/10.1007/s11071-022-07859-9

ORIGINAL PAPER

Anti-swing sliding mode control of three-dimensional double pendulum overhead cranes based on extended state observer

Qihang Guo · Lin Chai · Huikang Liu

Received: 28 February 2022 / Accepted: 27 August 2022 / Published online: 20 September 2022

Abstract When the double pendulum crane works in three-dimensional motion mode, it can significantly improve transportation efficiency. However, controlling the two-stage swing angles in the three-dimensional motion mode is complex and challenging. This paper presents a coordinated control method for the track and trolley of the double pendulum crane to improve the working efficiency of the crane, which realizes the anti-swing control of the double pendulum crane in three-dimensional movement mode. A three-dimensional double pendulum crane model is established, and the model is simplified by the differential flatness theory. A sliding mode control (SMC) method with an extended state observer (ESO) is designed to position and two-stage swing suppression of the three-dimensional double pendulum crane. For the actuator deadband, a transition process is introduced. The stability of the system is analyzed by the Lyapunov method. The proposed method has strong robustness and anti-interference ability. Theoretical and experimental results show that the proposed method can achieve fast and accurate positioning and effectively suppress the two-stage swing. This method is introduced into a nonlinear experimental platform. Compared with other technologies in the literature, the proposed method shortens the transit time, improves work efficiency, and reduces the safety risk.

Keywords Three-dimensional double pendulum crane · Anti-swing · Sliding mode · Differential flatness · Differential Tracker · Extended state observer

Q. Guo · L. Chai (✉) · H. Liu
College of Information Science and Engineering, Wuhan University of Science and Technology, Wuhan 430081, China
e-mail: 235126698@qq.com
Q. Guo
e-mail: gqh2020@wust.edu.cn
H. Liu
e-mail: huikangl@vip.sina.com

1 Introduction

The overhead crane is a piece of significant construction machinery and is widely used. Its good performance is essential to raise working efficiency. Especially when the cranes work in the three-dimensional motion mode, the transportation efficiency of the system will be significantly improved. However, the load will swing when the crane transports the load. In some cases, the movement of the crane presents a double pendulum effect [1]. In detail, the hook swings around the trolley while the load swings around the hook during the crane movement, which will reduce transportation efficiency and possibly cause safety problems. For these reasons, the elimination of swing in the transshipment of load has drawn the attention of researchers. The crane system is a typical underactuated system. Control variables are fewer than controlled variables. The underactuated system is nonlinear and has strong

coupling. Therefore, the control of a three-dimensional double pendulum crane system is challenging.

In recent years, the linear method and the sliding mode control method are the two widely-used solutions in practical applications due to the advantages of simplicity in structure. More specifically, the linear method refers to linearizing the crane model near the balance point [2–7], ignoring some specific nonlinear terms [8,9] and using various linear control methods to handle the simplified model. Based on the root locus and particle swarm optimization algorithm, several PID control methods are proposed [10,11]. However, traditional PID control is challenging to obtain expected control performance [12–18]. Hence, it needs to be combined with other control strategies, such as fuzzy control [12], neural network [13], multi-objective optimization algorithm [14–16], genetic algorithm [17,18], etc. The introduction of intelligent algorithms reduces the difficulty of parameter optimization and improves the convergence speed, accuracy, and reliability of optimization. Saeidi et al. [19] design a PID control method for a gantry crane system with precise positioning and anti-swing performance by neural network self-tuning technology. In addition to the above series of PID control methods, many linear ways are applied to the crane system. A status feedback controller is developed [20], which performs well on a crane in 3D motion mode. On this basis, a linear quadratic regulator (LQR) approach is proposed [21]. However, this method linearizes the crane system model without considering the nonlinear factors. In addition, researchers apply the local feedback linearization method to double-pendulum offshore boom crane system [22], three-dimensional motion mode crane system [23,24], and the crane system with load-lifting motion mode [25], respectively.

Actually, excellent robustness is expected for the crane control system when the parameters vary and external disturbances exist. The sliding control method has the benefits of simple implementation, fast response, and strong robustness to system parameter changes [26–38]. Therefore, it is suitable for all kinds of crane control systems such as second-order sliding mode control method of port crane system [26], sliding mode for unmatched disturbances system [27], an adaptive integral SMC method of port crane system [28], hierarchical sliding mode control method of bridge crane system [29,30], etc. In detail, a model-independent control method is proposed for the three-dimensional crane system [31]. It could realize the accurate positioning and swing suppression of the trolley. An adaptive sliding mode control is presented for two-stage swing bridge crane system [32]. It enables the system to enter the desired sliding surface as soon as possible and also improves the tracking accuracy of the trolley. In [33], a fuzzy-SMC method is designed for a finite time system. In [34], a global-equivalent SMC is designed for anti-swing control of the overhead crane. Combining the sliding control method with other control patterns, the researchers propose an enhanced coupling PD with sliding mode control method [35], adaptive sliding mode control method [36–38], etc.

In the actual operation of the crane, many physical quantities can not be measured directly, such as some state status of the crane, external disturbances, and additional noise from traditional sensors in the measurement process, which makes the closed-loop control of the system complex. In [39], a revolving scheme is proposed to solve the Abel Equation for a satellite rotation cascade, providing a good control idea to improve the crane's anti-swing control performance. In order to improve the anti-swing control effect of the crane, many scholars use the observer method to observe these state variables, which reduces the number of sensors and noise interference in the process of sensor measurement. An observer for the length of the sling rope is presented, which can observe the length of the sling rope [40]. This provides an effective anti-swing method for some workplaces where the change of the rope length is not easy to detect. A speed observer is designed to achieve the goal of effective positioning and swing suppression without requiring speed feedback, which achieves the accurate positioning of load when the ship crane is working at sea [41]. An extended state observer is designed in [42], and a disturbance observer is designed in [43].

Besides, to reduce the swing angle, scholars also propose many effective nonlinear control methods to suppress swing for three dimensional crane [44–52]. A new nonlinear time sub-optimal trajectory planning method is put forward, which can realize effective control of the crane without linearizing the original nonlinear dynamics [44]. A robust passivity-based adaptive control method is proposed for payload trajectory tracking of three-dimensional bridge cranes with variable length sling [45]. A robust finite-time anti-swing is designed for a 3-D crane, which works well even with parameter uncertainties [46]. In [47],

an important memory function is constructed featuring expected damping based on passivity. A nonlinear controller is delivered by enforcing the coupled dissipation inequality to suppress the swing angle of the crane. In [48], nonlinear motion control is established in three-dimensional boom cranes. A partial differential equation (PDE) model is constructed for a three-dimensional boom crane, and a boundary control scheme for suppressing the load swing is presented [49]. In [50], a new adaptive control method is proposed for a 3D bridge crane based on trajectory planning, which achieves asymmetric swing elimination and trolley positioning. An optimal control algorithm based on energy is proposed [51,52]. When designing the crane controller, the controller's failure should also be considered. Generally, the input amplitude can be controlled within the allowable range to avoid being saturated. The control rule based on the dissipation theory can be effectively applied to the rotating servo system, which provides a good control idea to prevent the crane system from getting into the saturation of the actuator [53]. For the input of the control system, a method of the transition process is designed to avoid the situation where the input to the system is too large, exceeding the limits of actuator control input [42].

All of above mentioned have achieved good positioning and anti-swing performance. However, in general, the above studies still have some deficiencies: (1) Most of the above research objects are with anti-swing control of single pendulum cranes in three-dimensional motion mode or double pendulum cranes in two-dimensional motion mode, three-dimensional double pendulum cranes are not taken into account. (2) Because the three-dimensional double pendulum cranes have more states variables, the coupling between the state variables is very strong, which makes the anti-swing control of the crane more challenging. (3) For the deadband problem of the controller, the traditional scheme is less discussed.

Given above problems, a sliding control mode (SMC) based on an extended state observer is provided in this paper to suppress the two-stage swing of the three-dimensional double pendulum crane. Firstly, the mechanics model of the three-dimensional double pendulum crane is built according to the Lagrange motion equation [54]. After that, the system is converted to one input and one output system by differential flattening method. The extended state observer (ESO) is used to monitor the condition of the crane. Simultaneously,

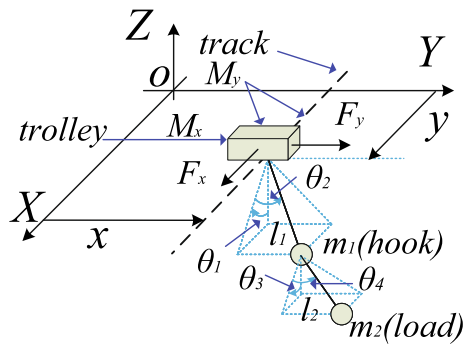

Fig. 1 Three-dimensional double pendulum crane model

the model error and system interference are estimated. SMC is used to obtain the crane control law. Finally, simulations and experiments verify the validity of the proposed approach.

The contribution of this paper is summarized as follows:

(1) Not merely the double pendulum but also the coordinated control of track and trolley motions are taken into account. The proposed nonlinear control method can accurately control the crane's movement and eliminate the load swing, which reduces the safety risk and improves transportation efficiency.
(2) Considering the actuator deadband, a transition process is introduced. By adjusting the control parameters, the deadband of the system's actuator could be avoided, which improves the system's operational performance.
(3) The method does not rely on the model parameters and has strong robustness and adaptability. The theoretical and experimental results verify the effectiveness of the proposed method.

The remainder of this paper is structured as follows: section II proposes the crane dynamic model and differential flattening. In section III, the control method is put forward. In section IV, the stability of the system is proved. In fifth section, a series of simulations and experiments based on this method verify the control performance of this method. The feasibility and validity of the control method are verified. The last section reviews the discussion of the whole article, summarizes the views of this article, and prospects the future research.

Table 1 Symbols and descriptions

Symbol	Description
M_x	Trolley mass
M_y	The total masses of trolley and track
m_1	Hook mass
m_2	Load mass
l_1	Rope length between the trolley and hook
l_2	String length between the hook and load
x	Trolley displacement in X direction
y	Trolley displacement in Y direction
Q_{kx}	External forces in the X direction
Q_{ky}	External forces in the Y direction
F_x	Driving force in the X direction
F_y	Driving force in the Y direction
df_x	Friction force in the X direction
df_y	Friction force in the Y direction
g	Gravitational acceleration

2 Crane model and differential flatness

2.1 Three-dimensional double pendulum crane model

During the working process of the crane, the load is transported to the specified location by the movement of the trolley, which requires not only accurate positioning but also as little oscillation as possible. In most crane models, the influence of friction force is ignored. However, the friction force of the crane is widespread in the actual construction process. Consequently, to increase the model's accuracy, a three-dimensional double pendulum overhead crane is built with a friction force effect. A three-dimensional double pendulum crane model is shown in Fig.1. Table 1 shows the symbols and descriptions of the model.

To simplify the description, the following concise symbols are used: $s_i = \sin\theta_i$, $c_i = \cos\theta_i$, $s_{i-j} = \sin(\theta_i - \theta_j)$, $c_{i-j} = \cos(\theta_i - \theta_j)$, $i, j = 1, 2, 3, 4 (i \neq j)$. Three-dimensional double pendulum crane mechanics model is established by Eqs. (1)–(6):

$$
\begin{aligned}
&(M_x + m_1 + m_2)\ddot{x} + \frac{m_1}{2}(-2s_1c_2l_1\dot{\theta}_1^2 - 2c_1s_2l_1\dot{\theta}_1\dot{\theta}_2 \\
&+2c_1c_2l_1\ddot{\theta}_1 - 2c_1s_2l_1\dot{\theta}_1\dot{\theta}_2 - 2s_1c_2l_1\dot{\theta}_2^2 \\
&-2s_1s_2l_1\ddot{\theta}_2) + \frac{m_2}{2}(-2s_1c_2l_1\dot{\theta}_1^2 - 2c_1s_2l_1\dot{\theta}_1\dot{\theta}_2 \\
&+2c_1c_2l_1\ddot{\theta}_1 - 2s_3c_4l_2\dot{\theta}_3^2 - 2c_3s_4l_2\dot{\theta}_3\dot{\theta}_4 \\
&+2c_3c_4l_2\ddot{\theta}_3 - 2c_1s_2l_1\dot{\theta}_1\dot{\theta}_2 - 2s_1c_2l_1\dot{\theta}_2^2 \\
&-2s_1s_2l_1\ddot{\theta}_2 - 2c_3s_4l_2\dot{\theta}_3\dot{\theta}_4 - 2s_3c_4l_2\dot{\theta}_4^2 \\
&-2s_3s_4l_2\ddot{\theta}_4) = Q_{kx}, \qquad (1)
\end{aligned}
$$

$$
\begin{aligned}
&(M_y + m_1 + m_2)\ddot{y} + m_1(-s_2l_1\dot{\theta}_2^2 + c_2l_1\ddot{\theta}_2) \\
&+m_2(-s_2l_1\dot{\theta}_2^2 + c_2l_1\ddot{\theta}_2 - s_4l_2\dot{\theta}_4^2 + c_4l_2\ddot{\theta}_4) = Q_{ky}, \qquad (2)
\end{aligned}
$$

$$
\begin{aligned}
&\frac{m_1}{2}(-4{l_1}^2c_2s_2\dot{\theta}_1\dot{\theta}_2 + 2{l_1}^2{c_2}^2\ddot{\theta}_1 - 2s_1c_2l_1\dot{\theta}_1\dot{x} \\
&-2c_1s_2l_1\dot{\theta}_2\dot{x} + 2c_1c_2l_1\ddot{x}) + \frac{m_2}{2}(-4{l_1}^2c_2s_2\dot{\theta}_1\dot{\theta}_2 \\
&+2{l_1}^2{c_2}^2\ddot{\theta}_1 + 2c_{1-3}(\dot{\theta}_1 - \dot{\theta}_3)c_2s_4l_1l_2\dot{\theta}_4 \\
&-2s_{1-3}s_2s_4l_1l_2\dot{\theta}_2\dot{\theta}_4 + 2s_{1-3}c_2c_4l_1l_2\dot{\theta}_4^2 \\
&+2s_{1-3}c_2s_4l_1l_2\ddot{\theta}_4 - 2s_{1-3}(\dot{\theta}_1 - \dot{\theta}_3)c_2c_4l_1l_2\dot{\theta}_3 \\
&-2c_{1-3}s_2c_4l_1l_2\dot{\theta}_2\dot{\theta}_3 - 2c_{1-3}c_2s_4l_1l_2\dot{\theta}_3\dot{\theta}_4 \\
&+2c_{1-3}c_2c_4l_1l_2\ddot{\theta}_3 - 2s_1c_2l_1\dot{\theta}_1\dot{x} \\
&-2c_1s_2l_1\dot{\theta}_2\dot{x} + 2c_1c_2l_1\ddot{x}) - \frac{m_1}{2}(-2s_1c_2l_1\dot{x}\dot{\theta}_1 \\
&-2c_1s_2l_1\dot{x}\dot{\theta}_2) - \frac{m_2}{2}(-2s_{1-3}s_2s_4l_1l_2\dot{\theta}_2\dot{\theta}_4 \\
&-2c_{1-3}s_2s_4l_1l_2\dot{\theta}_2\dot{\theta}_3 + 2c_{1-3}c_2s_4l_1l_2\dot{\theta}_1\dot{\theta}_4 \\
&-2s_{1-3}c_2c_4l_1l_2\dot{\theta}_1\dot{\theta}_3 - 2s_1c_2l_1\dot{x}\dot{\theta}_1 \\
&-2c_1s_2l_1\dot{x}\dot{\theta}_2) + (m_1 + m_2)gl_1s_1c_2 = 0, \qquad (3)
\end{aligned}
$$

$$
\begin{aligned}
&\frac{m_1}{2}(2{l_1}^2\ddot{\theta}_2 - 2c_1s_2l_1\dot{\theta}_1\dot{x} - 2s_1c_2l_1\dot{\theta}_2\dot{x} - 2s_1s_2l_1\ddot{x} \\
&-2s_2l_1\dot{y}\dot{\theta}_2 + 2c_2l_1\ddot{y}) + \frac{m_2}{2}(2{l_1}^2\ddot{\theta}_2 \\
&-2s_{1-3}(\dot{\theta}_1 - \dot{\theta}_3)s_2s_4l_1l_2\dot{\theta}_4 \\
&+2c_{1-3}c_2s_4l_1l_2\dot{\theta}_2\dot{\theta}_4 + 2c_{1-3}s_2c_4l_1l_2\dot{\theta}_4^2 \\
&+2c_{1-3}s_2s_4l_1l_2\ddot{\theta}_4 - 2c_{1-3}(\dot{\theta}_1 - \dot{\theta}_3)s_2s_4l_1l_2\dot{\theta}_3 \\
&+2s_{3-1}c_2s_4l_1l_2\dot{\theta}_2\dot{\theta}_3 + 2s_{3-1}s_2c_4l_1l_2\dot{\theta}_3\dot{\theta}_4 \\
&+2s_{3-1}s_2s_4l_1l_2\ddot{\theta}_3 - 2c_1s_2l_1\dot{\theta}_1\dot{x} - 2s_1c_2l_1\dot{\theta}_2\dot{x} \\
&-2s_1s_2l_1\ddot{x} - 2s_2c_4l_1l_2\dot{\theta}_2\dot{\theta}_4 - 2c_2s_4l_1l_2\dot{\theta}_4^2 \\
&+2c_2c_4l_1l_2\ddot{\theta}_4 - 2s_2l_1\dot{y}\dot{\theta}_2 + 2c_2l_1\ddot{y}) \\
&-\frac{m_1}{2}(-2{l_1}^2c_2s_2\dot{\theta}_1^2 - 2c_1s_2l_1\dot{\theta}_1\dot{x} - 2s_1c_2l_1\dot{\theta}_2\dot{x} \\
&-2s_2l_1\dot{y}\dot{\theta}_2) - \frac{m_2}{2}(2c_{1-3}c_2s_4l_1l_2\dot{\theta}_2\dot{\theta}_4
\end{aligned}
$$

$$
\begin{aligned}
&+2s_{3-1}c_2s_4l_1l_2\dot{\theta}_2\dot{\theta}_3 - 2{l_1}^2c_2s_2\dot{\theta}_1^2\\
&-2s_{1-3}s_2c_4l_1l_2\dot{\theta}_1\dot{\theta}_4 - 2c_{1-3}s_2c_4l_1l_2\dot{\theta}_1\dot{\theta}_3\\
&-2c_1s_2l_1\dot{\theta}_1\dot{x} - 2s_1c_2l_1\dot{\theta}_2\dot{x} - 2s_2c_4l_1l_2\dot{\theta}_2\dot{\theta}_4\\
&-2s_2l_1\dot{y}\dot{\theta}_2) + (m_1+m_2)gl_1c_1s_2 = 0, \qquad (4)\\
&\frac{m_2}{2}(2c_{3-1}(\dot{\theta}_3-\dot{\theta}_1)s_2s_4l_1l_2\dot{\theta}_2 + 2s_{3-1}c_2s_4l_1l_2\dot{\theta}_2^2\\
&+2s_{3-1}s_2c_4l_1l_2\dot{\theta}_2\dot{\theta}_4 + 2s_{3-1}s_2s_4l_1l_2\ddot{\theta}_2\\
&-2s_{1-3}(\dot{\theta}_1-\dot{\theta}_3)c_2c_4l_1l_2\dot{\theta}_1 - 2c_{1-3}s_2c_4l_1l_2\dot{\theta}_1\dot{\theta}_2\\
&-2c_{1-3}c_2s_4l_1l_2\dot{\theta}_1\dot{\theta}_4 + 2c_{1-3}c_2c_4l_1l_2\ddot{\theta}_1\\
&-4s_4c_4{l_2}^2\dot{\theta}_3\dot{\theta}_4 + 2{c_4}^2{l_2}^2\ddot{\theta}_3 - 2s_4c_3l_2\dot{x}\dot{\theta}_4\\
&-2c_4s_3l_2\dot{x}\dot{\theta}_3 + 2c_4c_3l_2\ddot{x})\\
&-\frac{m_2}{2}(2s_{1-3}s_2s_4l_1l_2\dot{\theta}_2\dot{\theta}_4 + 2c_{1-3}s_2s_4l_1l_2\dot{\theta}_2\dot{\theta}_3\\
&-2c_{1-3}c_2s_4l_1l_2\dot{\theta}_1\dot{\theta}_4 + 2s_{1-3}c_2c_4l_1l_2\dot{\theta}_1\dot{\theta}_3\\
&-2c_4s_3l_2\dot{x}\dot{\theta}_3 - 2s_4c_3l_2\dot{x}\dot{\theta}_4) + m_2gl_2c_4s_3 = 0, \qquad (5)\\
&\frac{m_2}{2}(-2s_{1-3}(\dot{\theta}_1-\dot{\theta}_3)s_2s_4l_1l_2\dot{\theta}_2 + 2c_{3-1}c_2s_4l_1l_2\dot{\theta}_2^2\\
&+2c_{3-1}s_2c_4l_1l_2\dot{\theta}_2\dot{\theta}_4 + 2c_{3-1}s_2s_4l_1l_2\ddot{\theta}_2\\
&+2c_{1-3}(\dot{\theta}_1-\dot{\theta}_3)c_2s_4l_1l_2\dot{\theta}_1 - 2s_{1-3}s_2s_4l_1l_2\dot{\theta}_1\dot{\theta}_2\\
&+2s_{1-3}c_2c_4l_1l_2\dot{\theta}_1\dot{\theta}_4 + 2s_{1-3}c_2s_4l_1l_2\ddot{\theta}_1 + 2{l_2}^2\ddot{\theta}_4\\
&-2s_4c_3l_2\dot{x}\dot{\theta}_3 - 2c_4s_3l_2\dot{x}\dot{\theta}_4 - 2s_4s_3l_2\ddot{x}\\
&-2s_2c_4l_1l_2\dot{\theta}_2^2 - 2c_2s_4l_1l_2\dot{\theta}_2\dot{\theta}_4 + 2c_2c_4l_1l_2\ddot{\theta}_2\\
&-2s_4l_2\dot{y}\dot{\theta}_4 + 2c_4l_2\ddot{y})\\
&-\frac{m_2}{2}(2c_{3-1}s_2c_4l_1l_2\dot{\theta}_2\dot{\theta}_4\\
&+2s_{1-3}c_2c_4l_1l_2\dot{\theta}_1\dot{\theta}_4\\
&-2c_{1-3}c_2s_4l_1l_2\dot{\theta}_1\dot{\theta}_3 - 2s_4c_4{l_2}^2\dot{\theta}_3^2 - 2s_4c_3l_2\dot{x}\dot{\theta}_3\\
&-2c_4s_3l_2\dot{x}\dot{\theta}_4 - 2c_2s_4l_1l_2\dot{\theta}_2\dot{\theta}_4\\
&-2s_4l_2\dot{y}\dot{\theta}_4)\\
&+m_2gl_2s_4c_3 = 0. \qquad (6)
\end{aligned}
$$

where M_x is the trolley mass, M_y is the sum of the masses of the trolley and the track, m_1 is the hook mass, m_2 is the load mass, x and y represent the trolley displacement in X and Y direction, l_1 refers to the rope length between the trolley and the hook, and l_2 is the string length between the hook and load.

Q_{kx} and Q_{ky} represent the crane system external forces in the X and Y directions.

$$Q_{kx} = F_x - df_x, \qquad (7)$$

$$Q_{ky} = F_y - df_y, \qquad (8)$$

where F_x, F_y are the system driving force in the X and Y directions, and the friction forces df_x and df_y are of the following form [3,4].

$$df_x = f_{r0}\tanh(\dot{x}/\xi) + k_f\dot{x} + k_r|\dot{x}|\dot{x}, \qquad (9)$$

$$df_y = f_{r0}\tanh(\dot{y}/\xi) + k_f\dot{x} + k_r|\dot{y}|\dot{y}, \qquad (10)$$

where f_{r0}, k_f and k_r are friction-related parameters and $\xi \in \mathbb{R}$ is a static friction coefficient. Suppose the crane has the following traits:

(1) Hook and load can be regarded as particles, and the masses and tension of the suspension rope and sling are negligible.
(2) When the crane is transporting goods, the goods oscillate around the equilibrium point, which swing angles are small enough, then the following assumptions can be made: $cos\theta_i \approx 1, sin\theta_i \approx \theta_i, \theta_i\theta_j \approx 0$, $\dot{\theta}_i\dot{\theta}_j \approx 0$, and $\theta_i\ddot{\theta}_j \approx 0$ ($i, j = 1, 2, 3, 4$) [2–9].
3) The coordinates of the starting point and endpoint of the crane are known.

Thus, the simplified model is Eqs. (11)–(16):

$$(M_x+m_1+m_2)\ddot{x} + m_1l_1\ddot{\theta}_1 + m_2(l_1\ddot{\theta}_1 + l_2\ddot{\theta}_3) = Q_{kx}, \qquad (11)$$

$$(M_y+m_1+m_2)\ddot{y} + m_1l_1\ddot{\theta}_2 + m_2(l_1\ddot{\theta}_2 + l_2\ddot{\theta}_4) = Q_{ky}, \qquad (12)$$

$$m_1({l_1}^2\ddot{\theta}_1 + l_1\ddot{x}) + m_2({l_1}^2\ddot{\theta}_1 + l_1l_2\ddot{\theta}_3 + l_1\ddot{x}) + (m_1+m_2)gl_1\theta_1 = 0, \qquad (13)$$

$$m_1({l_1}^2\ddot{\theta}_2 + l_1\ddot{y}) + m_2({l_1}^2\ddot{\theta}_2 + l_1l_2\ddot{\theta}_4 + l_1\ddot{y}) + (m_1+m_2)gl_1\theta_2 = 0, \qquad (14)$$

$$m_2(l_1l_2\ddot{\theta}_1 + {l_2}^2\ddot{\theta}_3 + l_2\ddot{x}) + m_2gl_2\theta_3 = 0, \qquad (15)$$

$$m_2({l_2}^2\ddot{\theta}_4 + l_1l_2\ddot{\theta}_2 + l_2\ddot{y}) + m_2gl_2\theta_4 = 0. \qquad (16)$$

2.2 Differential flatness determination

Substituting Eqs. (13) and (15) into Eqs. (17) and (18) yields:

$$\ddot{x} + l_1\ddot{\theta}_1 + \frac{m_2l_2}{m_1+m_2}\ddot{\theta}_3 + g\theta_1 = 0, \qquad (17)$$

$$\ddot{x} + l_1\ddot{\theta}_1 + l_2\ddot{\theta}_3 + g\theta_3 = 0. \qquad (18)$$

Define the displacement signal in the X direction as x_z,

$$x_z = x + l_1\theta_1 + l_2\theta_3. \qquad (19)$$

Combine Eq. (18) with Eq. (19), we can get

$$\theta_3 = -\frac{\ddot{x}_z}{g}. \qquad (20)$$

Further,

$$\dot{\theta}_3 = -\frac{x_z^{(3)}}{g}, \tag{21}$$

$$\ddot{\theta}_3 = -\frac{x_z^{(4)}}{g}. \tag{22}$$

Substituting Eqs. (20), (21), and (22) into Eqs. (17) and (18), we can get

$$\theta_1 = -\frac{\ddot{x}_z}{g} - \frac{m_1 l_2}{(m_1+m_2)g^2} x_z^{(4)}. \tag{23}$$

Then,

$$\dot{\theta}_1 = -\frac{x_z{}^{(3)}}{g} - \frac{m_1 l_2}{(m_1+m_2)g^2} x_z^{(5)}, \tag{24}$$

$$\ddot{\theta}_1 = -\frac{x_z{}^{(4)}}{g} - \frac{m_1 l_2}{(m_1+m_2)g^2} x_z^{(6)}. \tag{25}$$

Substituting Eqs. (20) and (23) into Eq. (19), horizontal travel x can be achieved as follows,

$$x = x_z + \frac{(l_1+l_2)}{g}\ddot{x}_z + \frac{m_1 l_1 l_2}{(m_1+m_2)g^2} x_z^{(4)}, \tag{26}$$

and then,

$$x^{(i)} = x_z{}^{(i)} + \frac{l_1+l_2}{g} x_z^{(i+2)} + \frac{m_1 l_1 l_2}{(m_1+m_2)g^2} x_z^{(i+4)}. \tag{27}$$

Similarly, the displacement signal in Y direction can be defined as y_z,

$$y_z = y + l_1\theta_2 + l_2\theta_4. \tag{28}$$

Further,

$$\theta_4 = -\frac{\ddot{y}_z}{g}, \tag{29}$$

$$\dot{\theta}_4 = -\frac{y_z^{(3)}}{g}, \tag{30}$$

$$\ddot{\theta}_4 = -\frac{y_z^{(4)}}{g}, \tag{31}$$

$$\theta_2 = -\frac{\ddot{y}_z}{g} - \frac{m_1 l_2}{(m_1+m_2)g^2} y_z^{(4)}, \tag{32}$$

$$\dot{\theta}_2 = -\frac{y_z{}^{(3)}}{g} - \frac{m_1 l_2}{(m_1+m_2)g^2} y_z^{(5)}, \tag{33}$$

$$\ddot{\theta}_2 = -\frac{y_z{}^{(4)}}{g} - \frac{m_1 l_2}{(m_1+m_2)g^2} y_z^{(6)}, \tag{34}$$

$$y^{(i)} = y_z{}^{(i)} + \frac{l_1+l_2}{g} y_z^{(i+2)} + \frac{m_1 l_1 l_2}{(m_1+m_2)g^2} y_z^{(i+4)}. \tag{35}$$

Any system of state variables can be expressed as algebraic forms x_z and y_z and their different order derivatives algebraic combinations. At this point, Eqs. (27) and (35) are single input single output (SISO) systems, where the system is not underactuated.

3 Control method

In the second section, the crane model is simplified, which may affect the model's accuracy. In this section, ESO will be introduced to observe the crane system's conditions. The initial conditions of the system are zero initial state. The error caused by inaccurate model and external interference will be equivalent to the total interference of the system for estimation. The error is compensated in the controller. In common control system, the error is directly referred to $e = v - y$, where v is the output of TD, and y stands for the system output. This error method makes the initial error very large and easy to overshoot, which is unreasonable. Depending on the carrying capacity of the controller, we organize a reasonable transition process. It can effectively solve the contradiction between the rapidity and overshoot of the control system, which is also an efficient means of improving the robustness of the regulator. For transition process, TD can produce a tracking and differential signal and filter out noise. On this basis, SMC is utilized to overcome system uncertainty.

According to the analysis in second section, the crane kinematics equations in the X and Y directions have the same structure, so this section only discusses the control strategy in the X-direction. The crane control system is displayed in Fig. 2. Figure 3 shows the sequence of the steps of the proposed method.

3.1 Design of ESO

Most control objects can be described as Eq. (36),

$$\begin{cases} x^{(n)} = f(x, \dot{x}, ...x^{(n-1)}, x^{(n)}, w(t), u, \dot{u}, \cdots, u^{(n)}, t) + bu \\ y = x(t). \end{cases} \tag{36}$$

where $w(t)$ refers to an unknown outer disturbance; u stands for plant input; the system order is n; b represents the control gain, $b > 0$; y denotes the system output; $x, \dot{x}, \ldots, x^{(n-1)}, x^{(n)}$ represent the system state variables and the n-order derivative of the value of the status; the $f(x, \dot{x}, \ldots, x^{(n-1)}, x^{(n)}, w(t), u, \dot{u}, \cdots, u^{(n)}, t)$ link to the outer disturbance denotes real-time

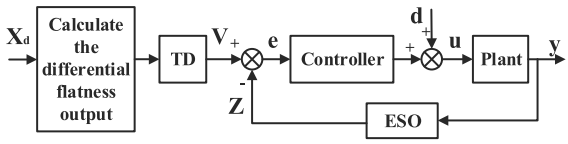

Fig. 2 Crane control system

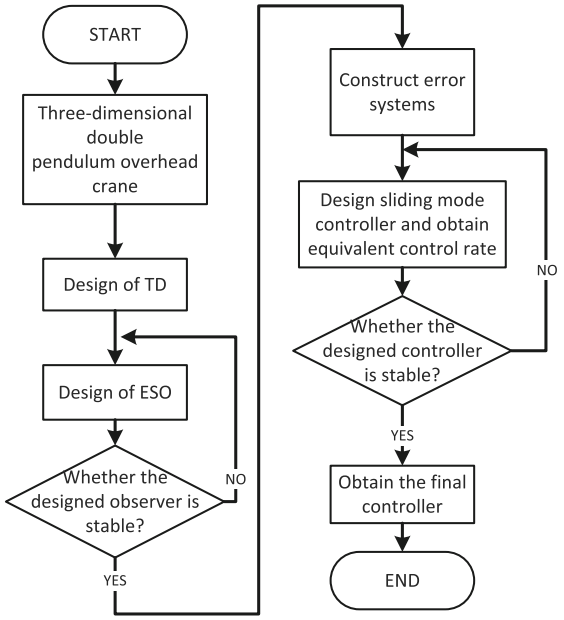

Fig. 3 Flowchart of the controller design

action, the system status and its derivatives are categorized as global disruption. For sake of expression, we shorten it as $f(X, \omega)$.

Next, a state of expansion $x_1, x_2, \cdots, x_{n+1}$ satisfy:

$$\begin{cases} \dot{x}_1 = x_2 \\ \dot{x}_2 = x_3 \\ \vdots \\ \dot{x}_{n-1} = x_n \\ \dot{x}_n = f(X, \omega) + bu \\ y = x_1, \end{cases} \tag{37}$$

$X = [x_1, x_2, \cdots, x_{n+1}]^{\mathrm{T}}$, e is observation error.

An ESO can be established as follows:

$$\begin{cases} e = z_1 - y_1 \\ \dot{z}_1 = z_2 - \beta_1 e \\ \dot{z}_2 = z_3 - \beta_2 e \\ \vdots \\ \dot{z}_{n-1} = z_n - \beta_{n-1} e \\ \dot{z}_n = -\beta_n e + bu. \end{cases} \tag{38}$$

z_i is the estimated value of $x_z^{(i-1)}$. β_i is the index of gain of the observer.

Once the control object presented in Eq. (36) is confirmed, the above function is available, and its derivative $\dot{f}(X, \omega)$ is obtained. Therefore, system state is depicted as Eq. (37).

Introducing the matrix,

$$A = \begin{bmatrix} 0\,1\,0\cdots 0 \\ 0\,0\,1\cdots 0 \\ 0\,0\,0\cdots 0 \\ 0\,0\,0\cdots 1 \\ 0\,0\,0\cdots 0 \end{bmatrix}, B = \begin{bmatrix} 0\cdots 0\,b\,0 \end{bmatrix}^{\mathrm{T}},$$

$$X = [x_1, x_2, \cdots, x_{n+1}]^{\mathrm{T}}.$$

Then, Eq. (37) can be expressed as,

$$\dot{X} = AX + Bu. \tag{39}$$

3.2 Design of TD

Develop a TD for flat input x_{zd}.

From Eq. (19),

$$x_{zd} = x_d + l_1\theta_{1d} + l_2\theta_{3d}. \tag{40}$$

In Eq. (38), x_d is the expected horizontal movement of the crane; θ_{1d} is the oscillating angle for the first stage, θ_{3d} stands for the desired second stage flip degree for the system, θ_{1d} and θ_{3d} are set to zero; therefore, Eq. (40) may be reduced to Eq. (41),

$$x_{zd} = x_d. \tag{41}$$

As a result, we can determine the formula for TD. It is designed as follows:

$$\begin{cases} \dot{v}_1 = v_2 \\ \dot{v}_2 = v_3 \\ \dot{v}_3 = v_4 \\ \dot{v}_4 = v_5 \\ \dot{v}_5 = v_6 \\ \dot{v}_6 = -r(r(r(r(r(r(v_1 - v_0) + 6v_2) + 15v_3) \\ +20v_4) + 15v_5) + 6v_6). \end{cases} \tag{42}$$

In Eq. (42), $v_0 = x_{zd}$ is the setting value of the displacement control, and v_1 corresponds to the transition process implemented by TD; v_2 refers to the differential of v_1; v_3 stands for the 2nd derivative of v_1; v_4 is the 3rd derivative of v_1; v_5 represents the 4th derivative of v_1; v_6 is the 5th derivative of v_1; r denotes an adjustment to TD's performance according to system requirements.

3.3 Design of SMC

The nonlinear factors ignored in modeling will affect the control effect of the system in practice, especially for external disturbances and parameter perturbations. SMC is robust to outer disturbances and parameter uncertainties. For the differential equation of motion Eq. (37), where the function $f(X, \omega)$ is known, and the coordinate of the system state variable $(x_1, x_2, \ldots, x_n)$ is the phase coordinate variable $(x, \dot{x}, \ldots, x^{(n-1)})$, then the tracking error and its derivatives are:

$$\begin{cases} e_1 = x_1 - x_{1d} \\ e_2 = x_2 - x_{2d} \\ e_3 = x_3 - x_{3d} \\ e_4 = x_4 - x_{4d} \\ e_5 = x_5 - x_{5d} \\ e_6 = x_6 - x_{6d} \\ \dot{e}_1 = \dot{x}_1 - \dot{x}_{1d} \\ \dot{e}_2 = \dot{x}_2 - \dot{x}_{2d} \\ \dot{e}_3 = \dot{x}_3 - \dot{x}_{3d} \\ \dot{e}_4 = \dot{x}_4 - \dot{x}_{4d} \\ \dot{e}_5 = \dot{x}_5 - \dot{x}_{5d} \\ \dot{e}_6 = \dot{x}_6 - \dot{x}_{6d}. \end{cases} \tag{43}$$

$x_{1d}, x_{2d}, x_{3d}, x_{4d}, x_{5d}$, and x_{6d} are ideal state variables.

The sliding surface can be designed:

$$s = c_1 e_1 + c_2 e_2 + \ldots + c_n e_n, \tag{44}$$

where c_i must satisfy the Hurwitz condition, then $c_i > 0$ $(i = 1, 2, ..., n)$. In general, $c_n = 1$ [55].

Combining Eqs. (37) and (44), one can get

$$\begin{aligned} \dot{s} &= c_1 \dot{e}_1 + c_2 \dot{e}_2 + \ldots + c_n \dot{e}_n \\ &= \sum_{i=2}^{n} c_{i-1} x_i + f(X, \omega) + bu \end{aligned} \tag{45}$$

The traditional sliding mode uses the discrete switch function. Some improved control strategies change the switch function to the saturation function, which reduces the amplitude of chattering brought by the saltation of the switch function to a certain extent. However, there is still a large amount of buffeting. The role of the hyperbolic tangent replaces the switching process to minimize the amplitude of oscillations caused by the switching function. The change of the procedure is smooth, and there is no sudden change, which weakens the high-frequency vibration of the sliding mode to a certain extent. The hyperbolic tangent function can be expressed as

$$\tanh(\alpha x) = \frac{e^{\alpha x} - e^{-\alpha x}}{e^{\alpha x} + e^{-\alpha x}}. \tag{46}$$

α is the weight factor and a positive value. The smaller α is, the greater the boundary layer thickness is, the slower the system convergence is, and the worse the system robustness is. When $\alpha \to +\infty$, it will be converted to the switching process, which will cause greater buffeting. In this paper, $\alpha = 2$ can meet the requirements of the accuracy and robustness of the system.

Then, the control rate u can be obtained:

$$u = -\frac{\sum_{i=2}^{n} c_{i-1} x_i + f(X, \omega)}{b} - \frac{\tanh(\alpha s)}{b}. \tag{47}$$

4 Stability analysis

To simplify analysis, we indicate the corresponding observation value x_i $(i = 1, 2, \ldots, n+1)$ as $\tilde{x}_i$ $(i = 1, 2, \ldots, n+1)$.

$$\dot{\tilde{X}} = A\tilde{X} + Bu + L(X - \tilde{X}). \tag{48}$$

A stands for extended observer observation vector. B is the optional observer's constant gain matrix.

$$L = \begin{bmatrix} l_1 & 0 \cdots 0 \\ l_2 & 0 \cdots 0 \\ \vdots & \vdots \ddots \vdots \\ l_{n+1} & 0 \cdots 0 \end{bmatrix}_{(n+1)\times(n+1).} \tag{49}$$

Subtract Eq. (48) from Eq. (39):

$$\dot{X} - \dot{\tilde{X}} = (A - L)(X - \tilde{X}). \tag{50}$$

For the observation error to be close to zero, the above system should meet the stability requirements. According to the stability condition of linear constant system, all the eigenvalues of the system matrix are in the left half-open complex plane [56]. That is, all the eigenvalues of matrix $[A - L]$ have negative part of the real roots, and the observer state $\tilde{X}$ will progressively approximate the actual state X.

Theorem 1 *With the control rate in Eq.* (47)*, the system is uniformly asymptotically stable at the equilibrium point.*

Proof From Eqs. (44) and (45), the Lyapunov function is defined as

Table 2 System model parameters

M_x[kg]	20	M_y[kg]	30	m_1[kg]	5	m_2[kg]	5	x_d[m]	1.5
l_1[m]	1	l_2[m]	0.5	g[m/ s^2]	9.8	y_d[m]	2	f_{r0}	4.4
k_f	0.05	k_r	0.45	ξ	0.01	–	–	–	–

$$V = \frac{1}{2}s^2, \tag{51}$$

$$\begin{aligned}\dot{V} &= s\dot{s} \\ &= s(c_1\dot{e}_1 + c_2\dot{e}_2 + \ldots + c_n\dot{e}_n) \\ &= s\left(\sum_{i=2}^{n} c_{i-1}x_i + f(X,\omega) + bu\right).\end{aligned} \tag{52}$$

Substituting Eq. (47) into Eq. (52):

$$\begin{aligned}\dot{V} &= s\dot{s} \\ &= s\left(\sum_{i=2}^{n} c_{i-1}x_i + f(X,\omega)\right. \\ &\quad \left. -b\left(\frac{\sum_{i=2}^{n} c_{i-1}x_i + f(X,\omega)}{b} + \frac{\tanh(\alpha s)}{b}\right)\right) \\ &= -s * \frac{\tanh(\alpha s)}{b},\end{aligned} \tag{53}$$

$$\dot{V} = s\dot{s} = -s * \frac{\tanh(\alpha s)}{b} \begin{cases} < 0, & s > 0 \\ = 0, & s = 0 \\ < 0, & s < 0 \end{cases}. \tag{54}$$

According to Lyapunov stability theory [57], one may obtain from Eqs. (47) and (54) that the system is uniformly asymptotically stable at equilibrium point. □

5 Simulations and experiments

In this section, some simulations and experiments are conducted to evaluate the effectiveness and robustness of the proposed method. For this purpose, the system parameters of the crane are set, and a set of control parameters of a three-dimensional double pendulum overhead crane are established. Based on these control parameters, the comparative simulation experiments of the crane are carried out. A comparative simulation experiment is established to study the error between the simplified model and the original model. The results indicate that the error between both models is less than 1%. Next, four robust experiments are conducted to evaluate the robustness and anti-interference ability. Then, a DSP-based experimental platform is developed to verify the proposed methods.

Table 3 Controller parameters

c_1	c_2	c_3	c_4	c_5	r_x	r_y	w_o
32	80	80	40	10	1.5	1.5	102

5.1 Simulation conditions

A simulation is conducted to estimate the controller control effectiveness in MATLAB/Simulink environment. Table 2 sets out the parameters of the system model.

In view of system control performance, the parameters of crane control system are shown in Table 3.

c_1–c_5 are the parameters of sliding mode controller, r_x and r_y are the parameters of TD, and w_o is the bandwidth of ESO, respectively.

5.2 Simulation comparison

In this part, the proposed control method is compared with two other typical control schemes. The PID control parameters are $kp_x = 6.667$, $ki_x = 0.0665$, $kd_x = 18.97$, $kp_{\theta 1} = 0.2778$, $ki_{\theta 1} = 6.606$, $kd_{\theta 1} = 12.54$, $kp_{\theta 3} = 0.334$, $ki_{\theta 3} = 1.333$, $kd_{\theta 3} = 1.81$, $kp_y = 3.33$, $ki_y = 0.067$, $kd_y = 19.06$, $kp_{\theta 2} = -0.036$, $ki_{\theta 2} = 6.22$, $kd_{\theta 2} = 20.83$, $kp_{\theta 4} = 0.334$, $ki_{\theta 4} = 1.999$, $kd_{\theta 4} = 1.808$.

The comparative simulation results are shown in Fig. 4. In Fig. 4, the maximum swing angles of several crane control methods are less than 10°, which verifies the correctness and rationality of hypothesis 2 in Sect. 2.1. From the results in Table 4, the control method proposed for the three-dimensional double pendulum crane in this article can reach a quick and precise position, and the two-stage swing is suppressed from the system. Even though the control structure of PID is relatively simple, the number of control parameters that need to be optimized is excessive, which leads to difficulty in choosing the optimal set of control parameters. However, due to its simple structure, PID is widely

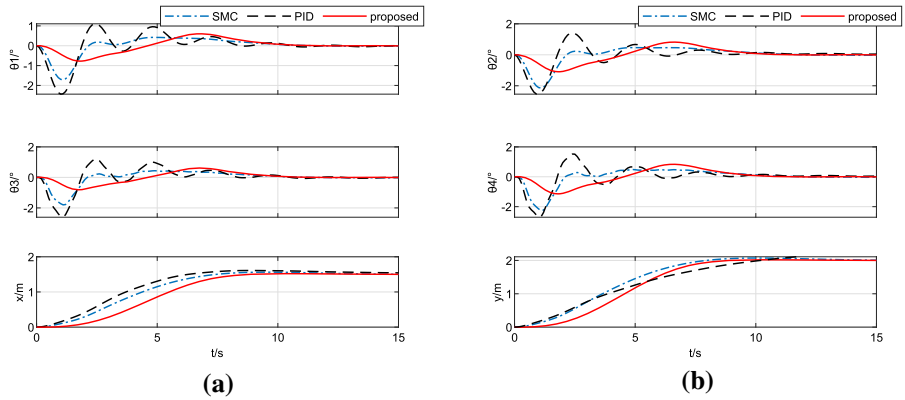

Fig. 4 Comparative control results: **a** X-direction; **b** Y-direction

Table 4 Comparative control results

Control method	$\theta_{1\max}$	$\theta_{2\max}$	$\theta_{3\max}$	$\theta_{4\max}$	θ_{res}	t_s
proposed	0.7759	1.096	0.8095	1.143	< 0.1	8.32
SMC	1.713	2.146	1.801	2.254	< 0.1	9.27
PID	2.439	2.541	2.611	2.707	< 0.1	10.13

used in industrial situations where the requirements of the swing angles are not very strict. The sliding mode control method has fewer parameters than PID, but the effect of sliding mode control is not as good as that of the strategy presented in this paper for swing elimination.

The crane model is simplified to reduce research difficulties, which may introduce model error. The extended state controller is introduced to estimate system state and model error. In order to investigate the relationship between simplified and original models, an experiment is conducted. The same control method and control parameters are used for experiments on both models in the simulation experiment. In Fig. 5, the error between the simplified model and the original model is below 1%.

From Fig. 5, the proposed control method achieves almost the same control effect on the original model as the simplified model, which manifests that the control method also applies to the nonlinear model. Therefore, the subsequent simulation experiments are based on the original model to study the proposed method's robustness.

By changing the parameter r of the TD, the influence of r on the control effect is studied. Fig. 6 shows the crane motion and its swing angles when $r = 1.2, r = 1.5, r = 1.8$. The simulation results indicate that the system's response speed increases as well as load swing with the rises of r. In addition, the control F varies with the adjustment of r. Therefore, r can be adjusted according to the actual control system requirements, such as controller deadband, maximum load swing angle limit, etc.

5.3 Robustness analysis

To investigate the robustness of the system when system parameters change, the following four groups of experiments are performed:

(1) When the load mass of the crane changes, the load mass increases from 5 to 10 kg and then to 20 kg.
(2) The rope length of the crane may change, increasing or decreasing by 50%.
(3) Change in the masses of track, trolley and hook on the crane.
(4) The crane may be interfered by external forces during operation, the system is disturbed by 10 N external forces in two directions.

In practice, the crane may transport the loads of different masses. Figure 7 shows the results of the system with varying the load mass. Even if the load mass increases fourfold, the proposed method can achieve accurate positioning and swing elimination for different loads masses without changing the control parameters. The results show that the crane can effectively prevent load swing when the mass of the load changes.

The rope length may change in different working places. In experiment 2, the influence of rope length change of crane on load anti-swing positioning is studied. Figure 8 shows the effect of the system when the

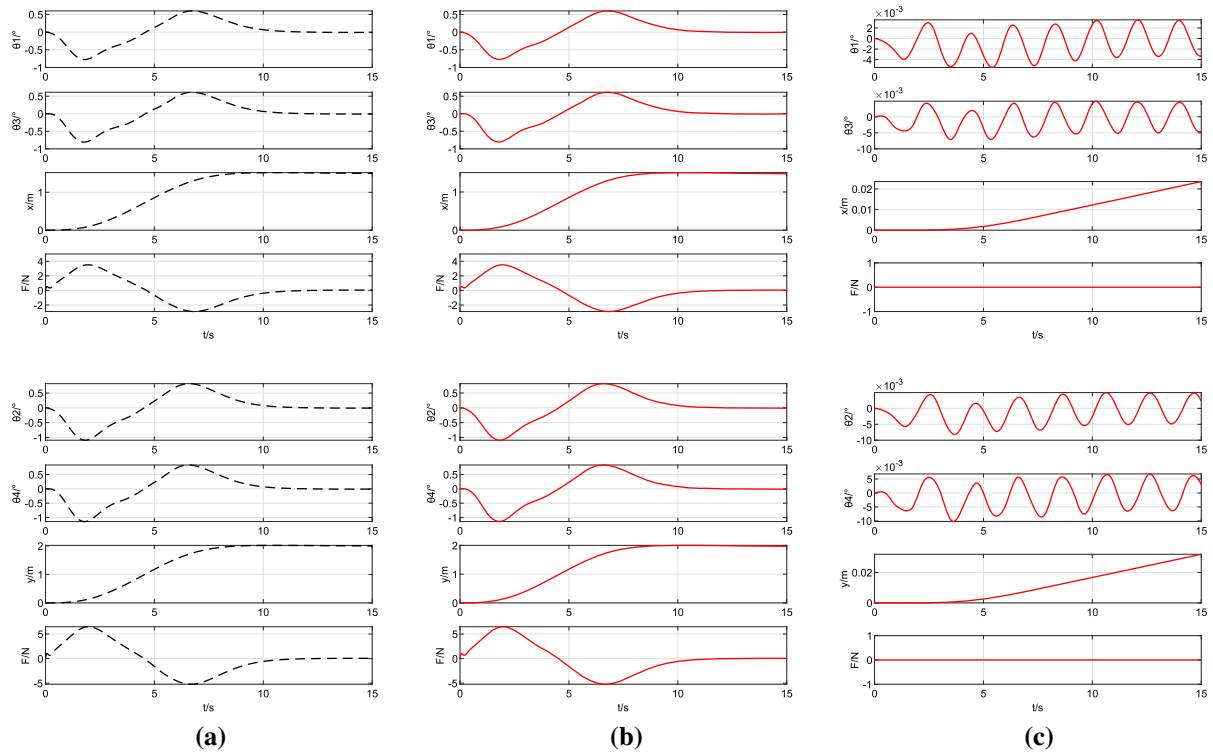

Fig. 5 Comparative simulation results between the proposed method with original model: **a** simplified model; **b** original model; **c** model error

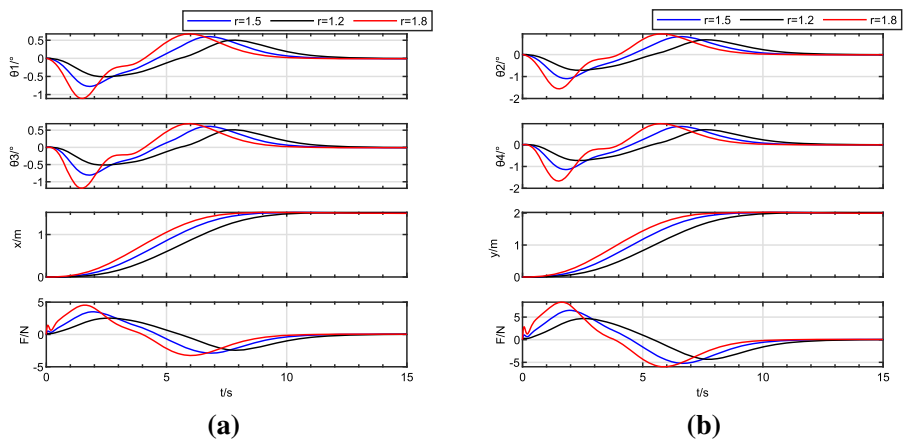

Fig. 6 Crane motion and swing angles when parameter r changes: **a** X-direction; **b** Y-direction

rope length changes. The results indicate that the system can effectively reduce load swing when rope length varies.

In most cases, the masses of track, trolley and hook of a crane system are fixed. To verify that the proposed control strategy does not depend on crane model parameters, the parameters shown in Table 2 are changed. Taking into account the following two situations:

S1: $M_x = 20\,\text{kg}$, $M_y = 30\,\text{kg}$, $m_1 = 5\,\text{kg}$, $m_2 = 5\,\text{kg}$.

S2: $M_x = 30\,\text{kg}$, $M_y = 40\,\text{kg}$, $m_1 = 10\,\text{kg}$, $m_2 = 5\,\text{kg}$.

From Fig. 9, the proposed method can effectively reduce the load swing when model parameters change considerably, which indicates that the method is insensitive to the model parameters.

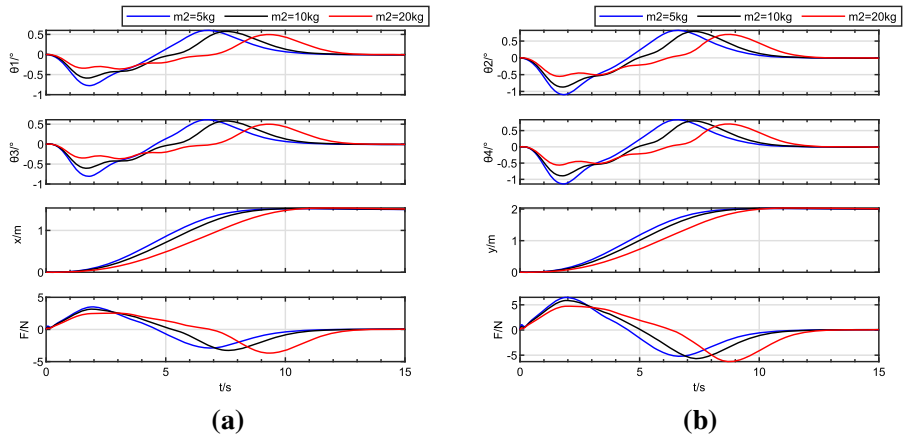

Fig. 7 Robust performance—crane motion and swing angles when parameter load mess varies: **a** X-direction; **b** Y-direction

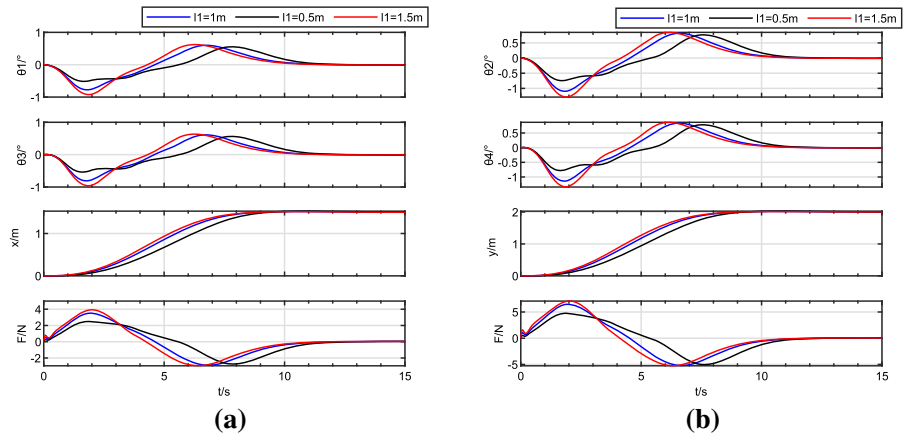

Fig. 8 Robust performance—crane motion and swing angles when parameter rope length varies: **a** X-direction; **b** Y-direction

External interference may occur during the operation of the crane. Considering the harsh working conditions, when the crane runs in the X direction, and at the 5th second, it is subject to intensity external interference of 0.1 s and 10 N. Running in the Y direction, and at the 6th second, it is subject to external interference of 10N for 0.1 s. Under such conditions, the anti-interference ability of the proposed control method is studied. Figure 10 shows the crane's operation under external impact in different directions and at other times. The result shows that the crane is not disturbed by the outside environment, proving that the proposed method has a solid anti-interference ability.

Nine groups of simulations are carried out in this section. A comparative experiment is conducted to evaluate crane operation performance among PID, SMC, and the method proposed in this article. The three control methods can realize no residual swing control of the crane. Compared with PID and SMC, the maximum swing angle of the proposed scheme can be reduced by 62% and 41%, and 17.88% and 10.24%, respectively, which can reduce the transportation time. These improve the crane's operational performance and reduce the possible risks. Comparing the original model with the simplified model, the control method functions well in the nonlinear and strongly coupled system. From the result, the error between the simplified model and the original is less than 1%, which indicates the simplification process is correct. The influence of parameter r in the TD on the system is studied. The parameter r can be adjusted according to actual control system requirements, such as controller deadband, maximum load swing angle limitation, etc. In addition, a series of robust experiments are established to prove that the proposed method has a solid anti-interference ability and high robustness.

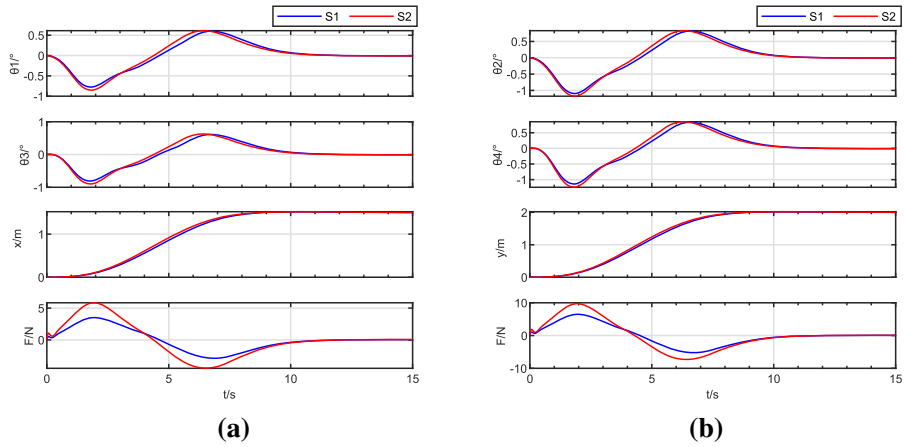

Fig. 9 Robust performance—crane motion and swing angles when the crane main parameters vary: **a** X-direction; **b** Y-direction

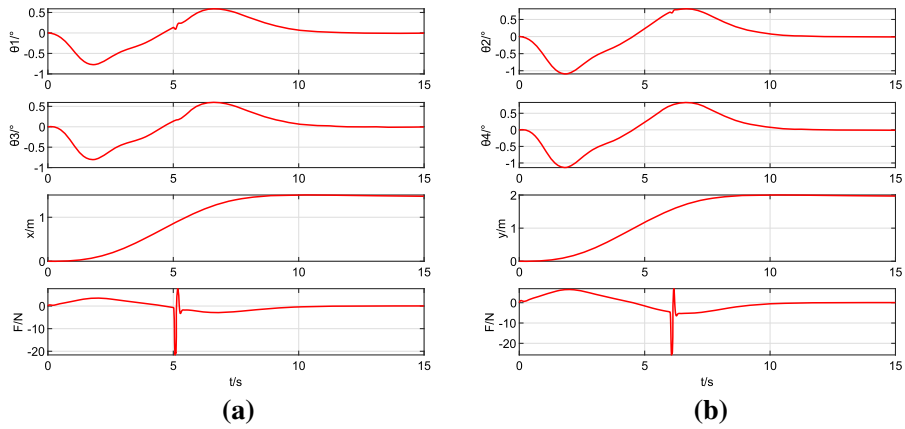

Fig. 10 Robust performance—external interference to the system: **a** X-direction; **b** Y-direction

5.4 Experiments and results analysis

As shown in Fig. 11, experiments are conducted in a three-dimensional double pendulum overhead crane platform (230 cm long × 180 cm wide × 120 cm high). The maximum length of lifting rope l_1 is 0.6 m and l_2 is 0.3 m. The maximum moving speed of the track and trolley is 0.4 m/s, the farthest displacement of track is 210cm, and the farthest displacement of trolley is 160 cm. The trolley and track driving motor are Inovance Servo Motor (AC 220V, 3000 rpm), a 20-bit incremental encoder, and the servo driver is Inovance IS620P servo drive. The main mechanical part of the three-dimensional double pendulum crane is composed of a truck and a trolley. The truck consists of a track and a trolley. Two AC motors provide driving forces in X and Y directions when transporting a load, respectively. The data feedback includes the position information and the hook and load swing angles. The encoder of the drive motor records the position information, and

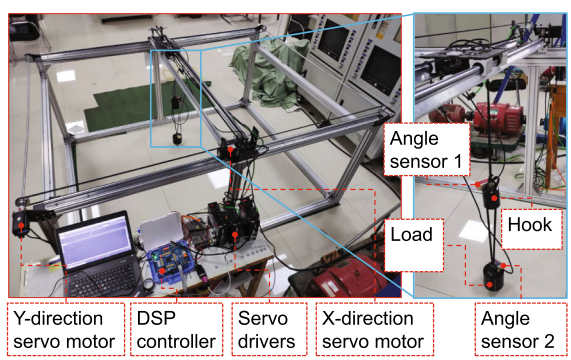

Fig. 11 Prototype crane

the angle sensors measure the swing angles information of the hook and the load.

The core of the whole control system is DSP (TEXAS INSTRUMENTS: TMS320F28335), which uses the communication protocol based on RS485 MODBUS RTU to communicate with the server drivers

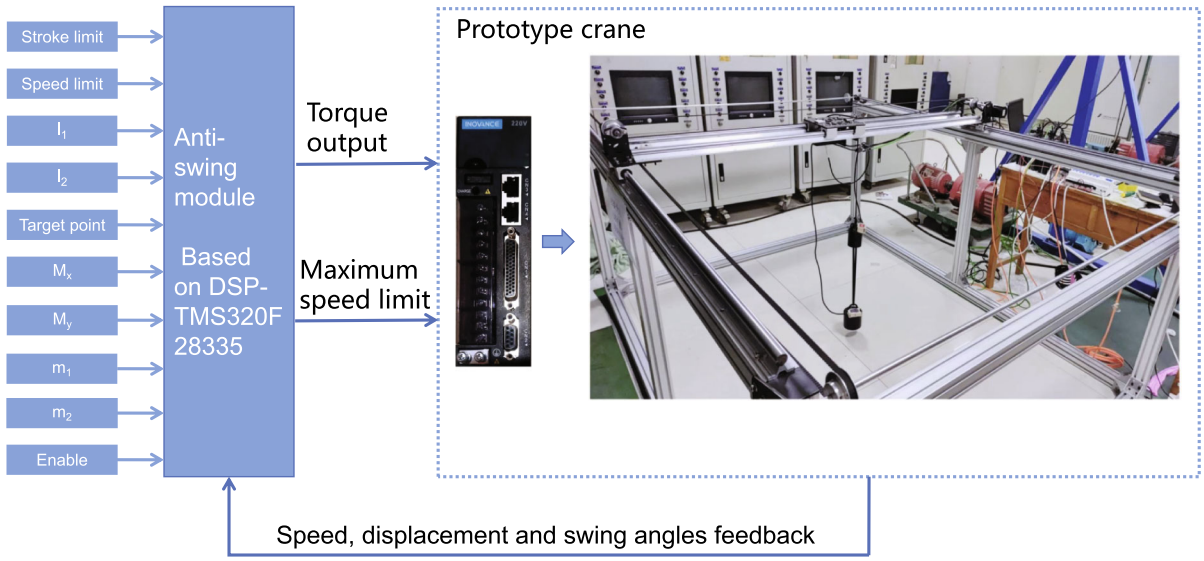

Fig. 12 Anti-swing module

Table 5 Experimental platform parameters

M_x[kg]	4.17	M_y[kg]	22.32	m_1[kg]	2.5
m_2[kg]	5	x_d[m]	1.5	y_d[m]	2
l_1[m]	0.6	l_2[m]	0.3	g[m/ s^2]	9.8

and the computer. Fig. 12 shows the anti-swing module. The main experimental steps are:

(1) The driver identifies the motor;
(2) Input crane and load parameters;
(3) Input the target point of the crane (take the current position of the crane as the coordinate origin) and enable the anti-swing module;
(4) The speed, displacement and swing angles of the crane in the experimental platform are fed back to the anti-swing module, which calculates and outputs the driving torque and maximum moving speed.

Table 5 sets out the parameters of the experimental platform. In Sect. 5.3, Fig. 9 shows that the proposed method can effectively reduce the load swing when model parameters change considerably. Therefore, the control parameters of the experimental platform use the parameters in Table 2.

To further evaluate the performance of the proposed controller, a control effect comparison among PID, SMC, energy-based control method [58], and the proposed method is depicted in Fig. 13. From the results in Table 6, the proposed method in this article can reach a quick and precise position, and the swing angles are the smallest among the four methods. Although the energy-based control method [58] achieves the shortest transportation time, in some industrial situations where the limit of load swing angle is stringent, such as the transportation of high-temperature molten metal, the transport speed requirements are relatively minor.

Table 6 Comparative control results

Control method	$\theta_{1\max}$	$\theta_{2\max}$	$\theta_{3\max}$	$\theta_{4\max}$	θ_{res}	t_s
Proposed	0.98	1.04	1.33	1.41	< 0.1	9.04
SMC	1.53	1.61	1.67	1.77	< 0.1	10.12
PID	2.08	2.13	2.37	2.55	< 0.1	11.21
Reference [58]	1.38	1.42	1.73	1.82	< 0.1	8.92

Two experiments corroborate the proposed method's robustness, including the change of rope length and load mass. From Figs.14 and 15, under the experimental platform, without adjusting the control parameters, the proposed method can suppress the load swing when the load mass and rope length vary.

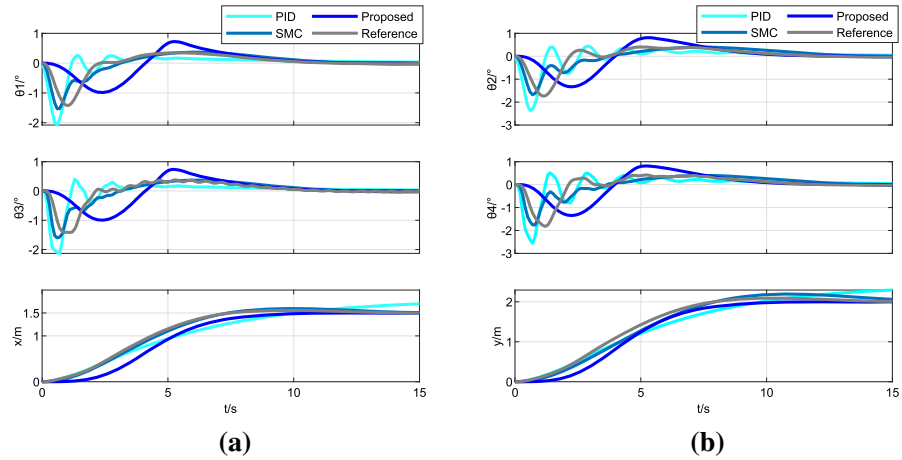

Fig. 13 Comparative experimental results of different methods: **a** X-direction; **b** Y-direction

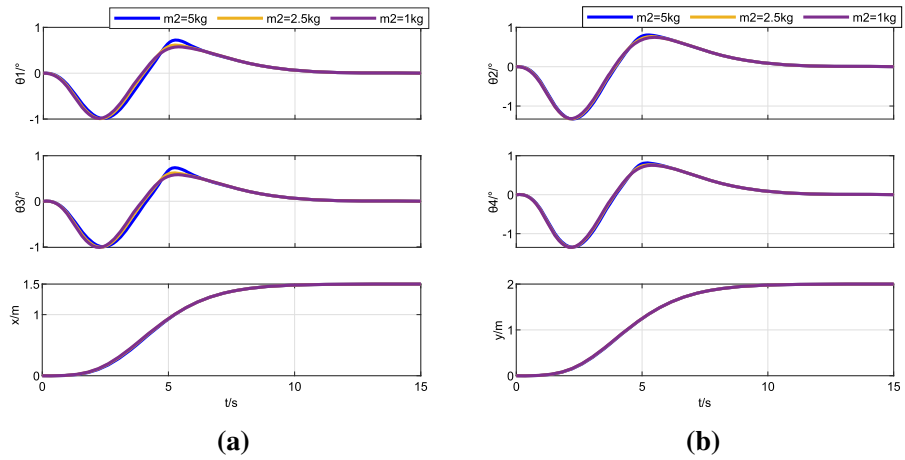

Fig. 14 Robust performance experiment—crane motion and swing angles when parameter load mess varies: **a** X-direction; **b** Y-direction

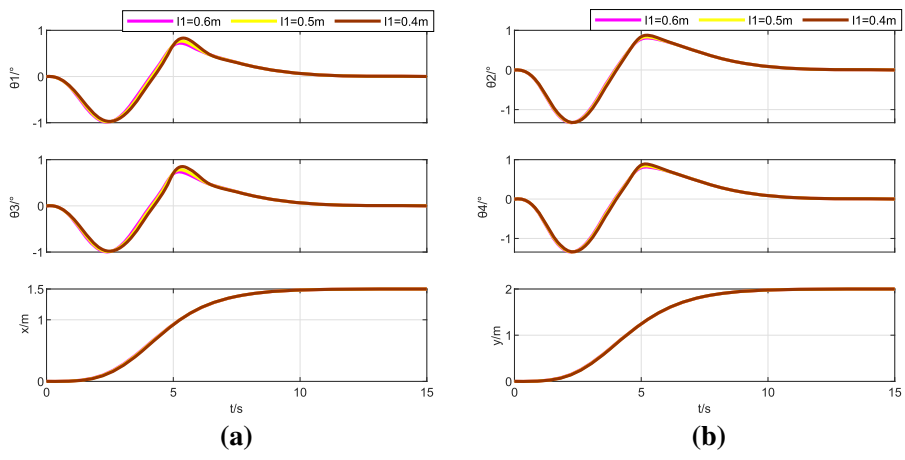

Fig. 15 Robust performance experiment—crane motion and swing angles when parameter rope length varies: **a** X-direction; **b** Y-direction

6 Conclusion

In actual industrial production, the double pendulum crane is widely used. Effective control of load swing during transportation significantly improves industrial production safety. The research on coordinated motion control of track and trolley of a double pendulum crane is of great significance to further improve the transportation efficiency of the crane. This paper proposes a sliding mode control based on an extended state observer to suppress the load swing for three-dimensional double-pendulum overhead cranes. Compared with other technologies in the literature, the proposed method shortens the transit time, improves work efficiency, and reduces the safety risk. The method is insensitive to the model parameters and has strong robustness. The proposed method is applied to a nonlinear experimental platform, and the theoretical and experimental results verify the effectiveness of the proposed method. The introduction of TD effectively solves the contradiction between the rapidity and overshoot of the control system. The problem of controller deadband saturation can be effectively solved. By adjusting the control parameters of TD, the problem of the system output caused by the observer delay error in the initial time can be effectively reduced. Restricted by experimental conditions, the effectiveness and accuracy of the proposed control method are validated in the laboratory at the present stage. The experiment has not been carried out under actual factory conditions. The anti-swing effect under factory conditions remains to be further studied. Currently, we are cooperating with a drive manufacturer to make the proposed control strategy for the general inverter and industrialize the proposed anti-swing strategy.

Acknowledgements This work was funded by the National Key R & D Program of China (Grant No. 2017YFC0805100).

Funding This work is supported by National Key R&D Program of China (2017YFC0805100).

Data availability The authors declare that the data supporting the findings of this study are available within the article.

Declarations

Conflict of interest The authors declare that there is no conflict of interests regarding the publication of this paper.

Appendix A : Observation effect of state observer

The overhead crane is a powerful engineering machine, and its working environment has unknown external interference and noise interference, which will affect the operating performance of the crane. In section III, an extended state observer is designed to observe these disturbances. The observations of these disturbances are introduced into the controller to enhance the anti-interference ability and robustness of the crane control system. The accuracy of the observed results directly affects the control effect of the controller. An experiment is performed on the ESO designed to detect the observer's observation effect in this section. The crane works in a noisy environment and, at the 5th second, suffers an external impact of 20N duration of 0.1s. Fig. 16 shows the observer's observations of a crane subjected to external disturbances of a size of 20N and duration of 0.1s. Fig. 17 shows the observer's ambient noise results. The ESO designed in this paper can effectively observe external disturbance and environmental noise from the observer's calculation speed and estimation accuracy. The introduction of the ESO enhances the stability and robustness of the system.

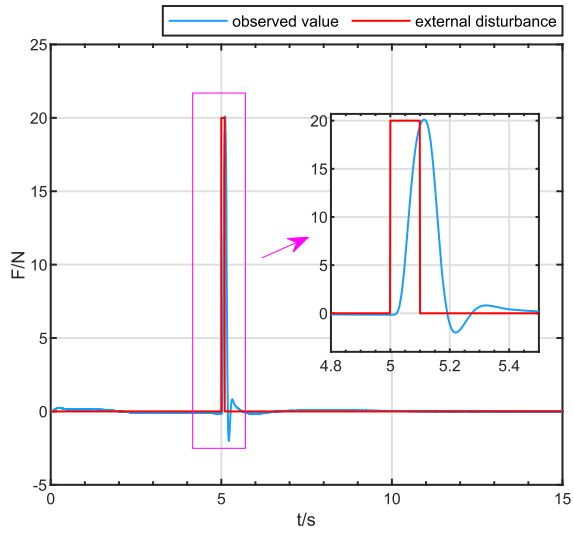

Fig. 16 Observation of external disturbance

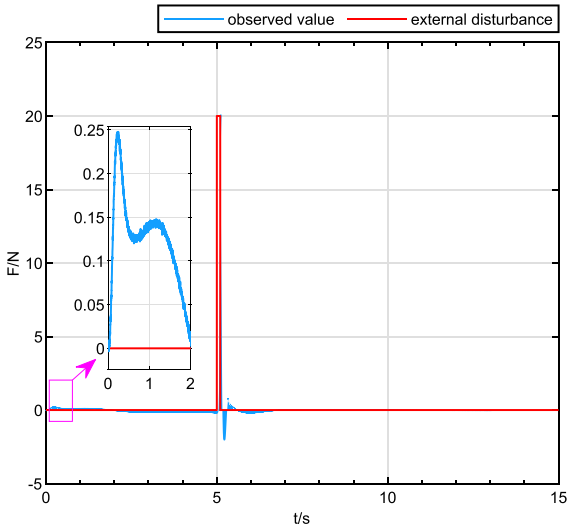

Fig. 17 Observation of ambient noise

Appendix B : Crane System Modeling

A three-dimensional double pendulum crane model is shown in Fig. 1. In the XYZ coordinate system, the trolley is located on the plane of XOY, trolley's coordinate is (x_M, y_M, z_M), hook's coordinate is $(x_{m_1}, y_{m_1}, z_{m_1})$, and load's coordinate is $(x_{m_2}, y_{m_2}, z_{m_2})$, where

$$\begin{cases} x_M = x \\ y_M = y \\ z_M = 0 \\ x_{m_1} = x + l_1 \sin\theta_1 \cos\theta_2 \\ y_{m_1} = y + l_1 \sin\theta_2 \\ z_{m_1} = -l_1 \cos\theta_1 \cos\theta_2 \\ x_{m_2} = x + l_1 \sin\theta_1 \cos\theta_2 + l_2 \sin\theta_3 \cos\theta_4 \\ y_{m_2} = y + l_1 \sin\theta_2 + l_2 \sin\theta_4 \\ z_{m_2} = -l_1 \cos\theta_1 \cos\theta_2 - l_2 \cos\theta_3 \cos\theta_4. \end{cases} \tag{55}$$

From the Eq. (55), the speed of the trolley is V_M, the speed of the hook is V_{m_1}, and the speed of the load is V_{m_2}, where

$$V_M = \begin{bmatrix} \frac{\partial}{\partial t} x(t) \\ \frac{\partial}{\partial t} y(t) \\ 0 \end{bmatrix} = \begin{bmatrix} \dot{x} \\ \dot{y} \\ 0 \end{bmatrix}, \tag{56}$$

$$\begin{aligned} V_{m_1} &= \begin{bmatrix} \frac{\partial}{\partial t} x(t) + l_1 c_2(t) \frac{\partial}{\partial t} s_1(t) + l_1 s_1(t) \frac{\partial}{\partial t} c_2(t) \\ l_1 \frac{\partial}{\partial t} s_2(t) + \frac{\partial}{\partial t} y(t) \\ -l_1 c_1(t) \frac{\partial}{\partial t} c_2(t) - l_1 c_2(t) \frac{\partial}{\partial t} c_1(t) \end{bmatrix} \\ &= \begin{bmatrix} \dot{x} + l_1 c_2 c_1 - l_1 s_1 s_2 \\ l_1 c_2 + \dot{y} \\ l_1 c_1 s_2 + l_1 c_2 s_1 \end{bmatrix}, \end{aligned} \tag{57}$$

$$\begin{aligned} V_{m_2} &= \begin{bmatrix} \frac{\partial}{\partial t} x(t) + l_1 c_2(t) \frac{\partial}{\partial t} s_1(t) + l_1 s_1(t) \frac{\partial}{\partial t} c_2(t) \\ + l_2 c_4(t) \frac{\partial}{\partial t} s_3(t) + l_2 s_3(t) \frac{\partial}{\partial t} c_4(t) \\ l_1 \frac{\partial}{\partial t} s_2(t) + l_2 \frac{\partial}{\partial t} s_4(t) + \frac{\partial}{\partial t} y(t) \\ -l_1 c_1(t) \frac{\partial}{\partial t} c_2(t) - l_1 c_2(t) \frac{\partial}{\partial t} c_1(t) \\ -l_2 c_3(t) \frac{\partial}{\partial t} c_4(t) - l_2 c_4(t) \frac{\partial}{\partial t} c_3(t) \end{bmatrix} \\ &= \begin{bmatrix} \dot{x} + l_1 c_2 c_1 - l_1 s_1 s_2 + l_2 c_4 c_3 - l_2 s_3 s_4 \\ l_1 c_2 + l_2 c_4 + \dot{y} \\ l_1 c_1 s_2 + l_1 c_2 s_1 + l_2 c_3 s_4 + l_2 c_4 s_3 \end{bmatrix}. \end{aligned} \tag{58}$$

From Eq.(56), Eq.(57), and Eq.(58), the system kinetic energy, T, is obtained as follows:

$$\begin{aligned} T &= \frac{M}{2} V_M^2 + \frac{m_1}{2} V_{m_1}^2 + \frac{m_2}{2} V_{m_2}^2 \\ &= \frac{M_x + m_1 + m_2}{2} \dot{x}^2 + \frac{M_y + m_1 + m_2}{2} \dot{y}^2 \\ &\quad + \frac{m_1}{2}(l_1^2 \dot{\theta}_2^2 + l_1^2 c_2^2 \dot{\theta}_1^2 \\ &\quad + 2 c_1 c_2 l_1 \dot{x} \dot{\theta}_1 - 2 s_1 s_2 l_1 \dot{x} \dot{\theta}_2 \\ &\quad + 2 c_2 l_1 \dot{y} \dot{\theta}_2) + \frac{m_2}{2}(l_1^2 \dot{\theta}_2^2 \\ &\quad + 2 c_{1-3} l_1 l_2 s_2 s_4 \dot{\theta}_2 \dot{\theta}_4 \\ &\quad + 2 s_{3-1} l_1 l_2 s_2 s_4 \dot{\theta}_2 \dot{\theta}_3 + l_1^2 c_2^2 \dot{\theta}_1^2 \\ &\quad + 2 s_{1-3} l_1 l_2 c_2 s_4 \dot{\theta}_1 \dot{\theta}_4 \\ &\quad + 2 c_{1-3} l_1 l_2 c_2 c_4 \dot{\theta}_1 \dot{\theta}_3 + 2 c_1 c_2 l_1 \dot{x} \dot{\theta}_1 \\ &\quad + l_2^2 \dot{\theta}_4^2 + c_4^2 l_2^2 \dot{\theta}_3^2 \\ &\quad + 2 c_3 c_4 l_2 \dot{x} \dot{\theta}_3 - 2 s_1 s_2 l_1 \dot{x} \dot{\theta}_2 - 2 s_3 s_4 l_2 \dot{x} \dot{\theta}_4 \\ &\quad + 2 l_1 l_2 c_2 c_4 \dot{\theta}_2 \dot{\theta}_4 + 2 c_2 l_1 \dot{y} \dot{\theta}_2 \\ &\quad + 2 c_4 l_2 \dot{y} \dot{\theta}_4). \end{aligned} \tag{59}$$

Taking trolley's plane as the zero potential energy plane, V which refers to the system's potential energy is obtained as follows:

$$V = -(m_1 + m_2) g l_1 c_1 c_2 - m_2 g l_2 c_3 c_4. \tag{60}$$

The Lagrange equation is a system of second-order differential equations,

$$\begin{cases} L(q, \dot{q}) = T(q, \dot{q}) - V(q, \dot{q}) \\ \frac{d}{dt}(\frac{\partial L}{\partial \dot{q}_k}) - \frac{\partial L}{\partial q_k} - Q_k = 0, \end{cases} \tag{61}$$

where L refers to Lagrange function; T represents system kinetic energy; V is system potential energy; q stands for Lagrange variable; Q_k refers to external forces.

Substituting Eq.(59) and Eq.(60) into Eq.(61), the three-dimensional double pendulum crane model (Eq.(1) - Eq.(6)) can be obtained.

References

1. Singhose, W., Kim, D., Kenison, M.: Input shaping control of double-pendulum bridge crane oscillations. J. Dyn. Syst. Meas. Control. Trans. ASME. (2008). https://doi.org/10.1115/1.2907363
2. Ouyang, H.M., Wang, J., Zhang, G.M., Mei, L., Deng, X.: Tracking and anti-sway control for double-pendulum rotary cranes using novel sliding mode algorithm. Zidonghua Xuebao/Acta Autom. Sin. **45**, 1344–1353 (2019). https://doi.org/10.16383/j.aas.c180452
3. Chen, H., Fang, Y., Sun, N.: A swing constrained time-optimal trajectory planning strategy for double pendulum crane systems. Nonlinear Dyn. **89**, 1513–1524 (2017). https://doi.org/10.1007/s11071-017-3531-0
4. Zhang, M., Ma, X., Chai, H., Rong, X., Tian, X., Li, Y.: A novel online motion planning method for double-pendulum overhead cranes. Nonlinear Dyn. **85**, 1079–1090 (2016). https://doi.org/10.1007/s11071-016-2745-x
5. Wu, Z., Xia, X., Zhu, B.: Model predictive control for improving operational efficiency of overhead cranes. Nonlinear Dyn. **79**, 2639–2657 (2015). https://doi.org/10.1007/s11071-014-1837-8
6. Chen, H., Fang, Y., Sun, N.: A swing constraint guaranteed MPC algorithm for underactuated overhead cranes. IEEE/ASME Trans. Mechatronics. **21**, 2543–2555 (2016). https://doi.org/10.1109/TMECH.2016.2558202
7. Ouyang, H.M., Wang, J., Zhang, G.M., Mei, L., Deng, X.: Trajectory generation for double-pendulum rotary crane. Kongzhi Lilun Yu Yingyong/Control Theory Appl. **36**, 1265–1274 (2019). https://doi.org/10.7641/CTA.2018.80454
8. Qian, D., Tong, S., Lee, S.G.: Fuzzy-Logic-based control of payloads subjected to double-pendulum motion in overhead cranes. Autom. Constr. **65**, 133–143 (2016). https://doi.org/10.1016/j.autcon.2015.12.014
9. Ouyang, H., Deng, X., Xi, H., Hu, J., Zhang, G., Mei, L.: Novel robust controller design for load sway reduction in double-pendulum overhead cranes. Proc. Inst. Mech. Eng. Part C J. Mech. Eng. Sci. **233**, 4359–4371 (2019). https://doi.org/10.1177/0954406218813383
10. Sun, N., Yang, T., Fang, Y., Wu, Y., Chen, H.: Transportation control of double-pendulum cranes with a nonlinear quasi-pid scheme: Design and experiments. IEEE Trans. Syst. Man Cybern. Syst. **49**, 1408–1418 (2019). https://doi.org/10.1109/TSMC.2018.2871627
11. Urbaś, A., Kłosiński, J., Augustynek, K.: The influence of the PID controller settings on the motion of a truck-mounted crane with a flexible boom and friction in joints. Control Eng. Pract. (2020). https://doi.org/10.1016/j.conengprac.2020.104610
12. Sun, Z., Ling, Y., Tan, X., Zhou, Y., Sun, Z.: Designing and application of type-2 fuzzy PID control for overhead crane systems. Int. J. Intell. Robot. Appl. **5**, 10–22 (2021). https://doi.org/10.1007/s41315-020-00157-w
13. Milovanović, M.B., Antić, D.S., Milojković, M.T., Nikolić, S.S., Perić, S.L., Spasić, M.D.: Adaptive PID control based on orthogonal endocrine neural networks. Neural Netwk. **84**, 80–90 (2016)
14. Li, H., Zhou, C., Lee, B.K., Lee, L.H., Chew, E.P., Goh, R.S.M.: Capacity planning for mega container terminals with multi-objective and multi-fidelity simulation optimization. IISE Trans. **49**, 849–862 (2017). https://doi.org/10.1080/24725854.2017.1318229
15. Khatir, S., Dekemele, K., Loccufier, M., Khatir, T., Abdel Wahab, M.: Crack identification method in beam-like structures using changes in experimentally measured frequencies and Particle Swarm Optimization. Comptes Rendus - Mec. **346**, 110–120 (2018). https://doi.org/10.1016/j.crme.2017.11.008
16. Cuong-Le, T., Minh, H. Le., Khatir, S., Wahab, M.A., Tran, M.T., Mirjalili, S.: A novel version of Cuckoo search algorithm for solving optimization problems. Expert Syst. Appl. (2021). https://doi.org/10.1016/j.eswa.2021.115669
17. Tiachacht, S., Bouazzouni, A., Khatir, S., Abdel Wahab, M., Behtani, A., Capozucca, R.: Damage assessment in structures using combination of a modified Cornwell indicator and genetic algorithm. Eng. Struct. **177**, 421–430 (2018). https://doi.org/10.1016/j.engstruct.2018.09.070
18. Abdel-razak, M.H., Ata, A.A., Mohamed, K.T., Haraz, E.H.: Proportional-integral-derivative controller with inlet derivative filter fine-tuning of a double-pendulum gantry crane system by a multi-objective genetic algorithm. Eng. Optim. **52**, 527–548 (2020). https://doi.org/10.1080/0305215X.2019.1603300
19. Saeidi, H., Naraghi, M., Raie, A.A.: A neural network self tuner based on input shapers behavior for anti sway system of gantry cranes. JVC/Journal Vib. Control. **19**, 1936–1949 (2013). https://doi.org/10.1177/1077546312453065
20. Ouyang, H., Zhang, G., Mei, L., Deng, X., Wang, D.: Load vibration reduction in rotary cranes using robust two-degree-of-freedom control approach. Adv. Mech. Eng. **8**, 1–11 (2016). https://doi.org/10.1177/1687814016641819
21. Shao, X., Zhang, J., Zhang, X.: Takagi-sugeno fuzzy modeling and PSO-Based Robust LQR anti-swing control for overhead crane. Math. Probl. Eng. (2019). https://doi.org/10.1155/2019/4596782
22. Li, Z., Ma, X., Li, Y.: Anti-swing control for a double-pendulum offshore boom crane with ship roll and heave movements. In: IEEE International Conference on Control and Automation, ICCA. pp. 165–170 (2020).https://doi.org/10.1109/ICCA51439.2020.9264524
23. Wu, X., He, X.: Partial feedback linearization control for 3-D underactuated overhead crane systems. ISA Trans. **65**, 361–370 (2016). https://doi.org/10.1016/j.isatra.2016.06.015
24. Huang, J., Zhu, K.: Dynamics and control of three-dimensional dual cranes transporting a bulky payload. Proc. Inst. Mech. Eng. Part C J. Mech. Eng. Sci. **235**, 1956–1965 (2021). https://doi.org/10.1177/0954406220949579
25. Lu, B., Fang, Y., Sun, N.: Enhanced-coupling adaptive control for double-pendulum overhead cranes with payload hoisting and lowering. Automatica. **101**, 241–251 (2019). https://doi.org/10.1016/j.automatica.2018.12.009
26. Shehu, M.A., Li, A.J., Tian, H.: Modified Higher-Order Sliding Mode Observer-Based Super-Twisting Controller for Perturbed Overhead Cranes. In: Proceedings - 2019 Chinese Automation Congress, CAC 2019. pp. 255–260. IEEE (2019).https://doi.org/10.1109/CAC48633.2019.8997439

27. Lu, B., Fang, Y., Sun, N.: Sliding mode control for underactuated overhead cranes suffering from both matched and unmatched disturbances. Mechatronics. **47**, 116–125 (2017). https://doi.org/10.1016/j.mechatronics.2017.09.006
28. Zhang, M., Zhang, Y., Ouyang, H., Ma, C., Cheng, X.: Adaptive integral sliding mode control with payload sway reduction for 4-DOF tower crane systems. Nonlinear Dyn. **99**, 2727–2741 (2020). https://doi.org/10.1007/s11071-020-05471-3
29. Le, H.X., Nguyen, T. Van., Le, A.V., Phan, T.A., Nguyen, N.H., Phan, M.X.: Adaptive hierarchical sliding mode control using neural network for uncertain 2D overhead crane. Int. J. Dyn. Control. **7**, 996–1004 (2019). https://doi.org/10.1007/s40435-019-00524-x
30. Liang, X., Fang, Y., Sun, N., Lin, H., Zhao, X.: Adaptive nonlinear hierarchical control for a rotorcraft transporting a cable-suspended payload. IEEE Trans. Syst. Man, Cybern. Syst. **51**, 4171–4182 (2021). https://doi.org/10.1109/TSMC.2019.2931812
31. Zhang, M., Zhang, Y., Chen, H., Cheng, X.: Model-independent PD-SMC method with payload swing suppression for 3D overhead crane systems. Mech. Syst. Signal Process. (2019). https://doi.org/10.1016/j.ymssp.2019.04.046
32. Gu, X., Xu, W., Zhang, M., Zhang, W., Wang, Y., Chen, T.: Adaptive controller design for overhead cranes with moving sliding surface. In: Chinese Control Conference, CCC. pp. 2412–2417 (2019).https://doi.org/10.23919/ChiCC.2019.8865222
33. Nguyen, V.T., Yang, C., Du, C., Liao, L.: Design and implementation of finite time sliding mode controller for fuzzy overhead crane system. ISA Trans. **124**, 374–385 (2022). https://doi.org/10.1016/j.isatra.2019.11.037
34. Wang, T., Tan, N., Qiu, J., Yu, Y., Zhang, X., Zhai, Y., Labati, R.D., Piuri, V., Scotti, F.: Global-Equivalent Sliding Mode Control Method for Bridge Crane. IEEE Access. **9**, 160372–160382 (2021). https://doi.org/10.1109/ACCESS.2021.3115164
35. Zhang, M., Zhang, Y., Cheng, X.: An Enhanced Coupling PD with Sliding Mode Control Method for Underactuated Double-pendulum Overhead Crane Systems. Int. J. Control. Autom. Syst. **17**, 1579–1588 (2019). https://doi.org/10.1007/s12555-018-0646-0
36. Kim, G.H., Hong, K.S.: Adaptive Sliding-Mode Control of an Offshore Container Crane with Unknown Disturbances. IEEE/ASME Trans. Mechatronics. **24**, 2850–2861 (2019). https://doi.org/10.1109/TMECH.2019.2946083
37. Zhang, M., Zhang, Y., Cheng, X.: Model-free adaptive integral sliding mode control for 4-DOF tower crane systems. In: IEEE/ASME International Conference on Advanced Intelligent Mechatronics, AIM. pp. 708–713 (2019). https://doi.org/10.1109/AIM.2019.8868534
38. Ouyang, H., Wang, J., Zhang, G., Mei, L., Deng, X.: Novel adaptive hierarchical sliding mode control for trajectory tracking and load sway rejection in double-pendulum overhead cranes. IEEE Access. **7**, 10353–10361 (2019). https://doi.org/10.1109/ACCESS.2019.2891793
39. Ershkov, S.V.: Revolving scheme for solving a cascade of Abel equations in dynamics of planar satellite rotation. Theor. Appl. Mech. Lett. **7**, 175–178 (2017). https://doi.org/10.1016/j.taml.2017.05.005
40. Wu, Q., Wang, X., Hua, L., Xia, M.: Modeling and nonlinear sliding mode controls of double pendulum cranes considering distributed mass beams, varying roped length and external disturbances. Mech. Syst. Signal Process. (2021). https://doi.org/10.1016/j.ymssp.2021.107756
41. Sun, N., Yang, T., Chen, H., Fang, Y.: Dynamic feedback antiswing control of shipboard cranes without velocity measurement: Theory and hardware experiments. IEEE Trans. Ind. Informatics. **15**, 2879–2891 (2019). https://doi.org/10.1109/TII.2018.2878935
42. Chai, L., Guo, Q., Liu, H., Ding, M.: Linear Active Disturbance Rejection Control for Double-Pendulum Overhead Cranes. IEEE Access. **9**, 52225–52237 (2021). https://doi.org/10.1109/ACCESS.2021.3070048
43. Miranda-Colorado, R.: Robust observer-based anti-swing control of 2D-crane systems with load hoisting-lowering. Nonlinear Dyn. **104**, 3581–3596 (2021). https://doi.org/10.1007/s11071-021-06443-x
44. Yang, T., Sun, N., Chen, H., Fang, Y.: Motion Trajectory-Based Transportation Control for 3-D Boom Cranes: Analysis, Design, and Experiments. IEEE Trans. Ind. Electron. **66**, 3636–3646 (2019). https://doi.org/10.1109/TIE.2018.2853604
45. Shen, P.Y., Schatz, J., Caverly, R.J.: Passivity-based adaptive trajectory control of an underactuated 3-DOF overhead crane. Control Eng. Pract. (2021). https://doi.org/10.1016/j.conengprac.2021.104834
46. Chwa, D.: Sliding-Mode-Control-Based Robust Finite-Time Antisway Tracking Control of 3-D Overhead Cranes. IEEE Trans. Ind. Electron. **64**, 6775–6784 (2017). https://doi.org/10.1109/TIE.2017.2701760
47. Zhang, M., Ma, X., Rong, X., Tian, X., Li, Y.: Nonlinear coupling control method for underactuated three-dimensional overhead crane systems under initial input constraints. Trans. Inst. Meas. Control. **40**, 413–424 (2018). https://doi.org/10.1177/0142331216658949
48. Sun, N., Yang, T., Fang, Y., Lu, B., Qian, Y.: Nonlinear Motion Control of Underactuated Three-Dimensional Boom Cranes with Hardware Experiments. IEEE Trans. Ind. Informatics. **14**, 887–897 (2018). https://doi.org/10.1109/TII.2017.2754540
49. Xing, X., Liu, J.: Vibration and position control of overhead crane with three-dimensional variable length cable subject to input amplitude and rate constraints. IEEE Trans. Syst. Man, Cybern. Syst. **51**, 4127–4138 (2021). https://doi.org/10.1109/TSMC.2019.2930815
50. Li, X., Geng, Z.: A novel trajectory planning-based adaptive control method for 3-D overhead cranes. Int. J. Syst. Sci. **49**, 3332–3345 (2018). https://doi.org/10.1080/00207721.2018.1537412
51. Zhang, S., He, X., Chen, Q.: Energy coupled-dissipation control for 3-dimensional overhead cranes. Nonlinear Dyn. **99**, 2097–2107 (2020). https://doi.org/10.1007/s11071-019-05451-2
52. Wu, X., He, X.: Nonlinear Energy-Based Regulation Control of Three-Dimensional Overhead Cranes. IEEE Trans. Autom. Sci. Eng. **14**, 1297–1308 (2017). https://doi.org/10.1109/TASE.2016.2542105
53. Manivannan, R., Samidurai, R., Cao, J., Perc, M.: Design of Resilient Reliable Dissipativity Control for Systems with Actuator Faults and Probabilistic Time-Delay Sig-

nals via Sampled-Data Approach. IEEE Trans. Syst. Man, Cybern. Syst. **50**, 4243–4255 (2020). https://doi.org/10.1109/TSMC.2018.2846645
54. Leshchenko, D., Ershkov, S., Kozachenko, T.: Evolution of a heavy rigid body rotation under the action of unsteady restoring and perturbation torques. Nonlinear Dyn. **103**, 1517–1528 (2021). https://doi.org/10.1007/s11071-020-06195-0
55. Ji, N., Liu, J., Yang, H.: Sliding mode control based on RBF neural network for a class of underactuated systems with unknown sensor and actuator faults. Int. J. Syst. Sci. **51**, 3539–3549 (2020). https://doi.org/10.1080/00207721.2020.1817615
56. Narendra, K.S., Balakrishnan, J.: A Common Lyapunov Function For Stable Lti Systems With Commuting A-Matrices. IEEE Trans. Automat. Contr. **39**, 2469–2471 (1994). https://doi.org/10.1109/9.362846
57. Kalman, R.E., Bertram, J.E.: Control system analysis and design via the "second method" of lyapunov: I continuous-time systems. J. Fluids Eng. Trans. ASME. **82**, 371–393 (1960). https://doi.org/10.1115/1.3662604
58. Ouyang, H., Zhao, B., Zhang, G.: Swing reduction for double-pendulum three-dimensional overhead cranes using energy-analysis-based control method. Int. J. Robust Nonlinear Control. **31**, 4184–4202 (2021). https://doi.org/10.1002/rnc.5466